Rare decays at Belle and Belle II

Seema Choudhury[a,*]

[a]*Iowa State University, USA*

E-mail: cseema@iastate.edu

We present the recent results of the rare decays from the Belle and Belle II experiments, collected at the $\Upsilon(4S)$ resonance. The data sample from Belle is 711 fb^{-1}, and 189 fb^{-1} or 361 fb^{-1} data sample from Belle II. Here, we report five rare decays involving $b \to s(d)$ transitions. The measurement of branching fractions for $B \to K^* \ell\ell$ decays using 189 fb^{-1} data sample from Belle II is consistent with the world averages. The best upper limits for lepton-flavor-violating $B^+ \to K^+ \tau\ell$ decays using Belle data sample, which are $< (0.59 - 2.45) \times 10^{-5}$ at 90% confidence level. The first ever search for $B^0 \to K^{*0} \tau\tau$ decay at Belle and the 90% confidence level upper limit is $< 3.1 \times 10^{-3}$. Belle II has measured the photon-energy spectrum in radiative B decays into inclusive final states involving hadron and a photon using 189 fb^{-1} data sample. The branching fraction measurements for different photon energy bins are consistent with the world averages. The measurement of branching fraction, isospin asymmetry, and CP-asymmetry for the exclusive $B \to \rho\gamma$ decay using combined data samples from Belle and Belle II are most precise to date.

---

*Speaker

1. Introduction

The rare decays which involves $b \rightarrow s(d)$ quark level transitions are flavor changing neutral current processes. These decays are forbidden at the tree level in the standard model (SM) and occur through electroweak loop diagrams, shown in Figure 1. The decays are highly suppressed, and
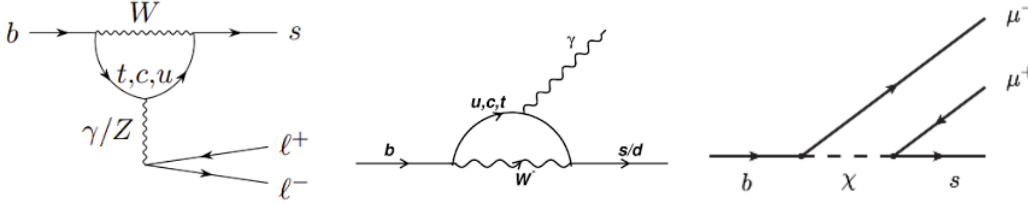

Figure 1: SM $b \rightarrow s\ell\ell$ (left), $b \rightarrow s\gamma$ (middle), and beyond SM $b \rightarrow s\ell\ell$ (right) transitions.

resulting branching ratio (BR) in SM is $O(10^{-7} - 10^{-4})$. The amplitude from the new physics (NP) contribution can interfere with the SM amplitude, altering physics observables like total or differential branching fraction, lepton-flavor universality ratio, isospin asymmetry, forward-background asymmetry, and angular observables etc. Therefore, there is many opportunities to probe the SM and explore the physics beyond the SM.

2. Belle and Belle II

The Belle [1] and Belle II [2] are asymmetric energy e^+e^- colliders, having center of mass energy at $\Upsilon(4S)$ resonance. The e^+ and e^- energies are 3.5 GeV and 8 GeV for Belle, and 4 GeV and 8 GeV for Belle II. Belle has collected 711 fb^{-1} data sample at $\Upsilon(4S)$ resonance and total recorded data from 1999 – 2010 is 1 ab^{-1}. Belle II started data taking from 2019 and so far it has collected 362 fb^{-1} data sample at $\Upsilon(4S)$ resonance and total recorded data is 424 fb^{-1} from 2019–2022. This recorded data is equivalent to BaBar data sample and half of Belle data sample. Belle II aims at collecting multi-ab^{-1} of data.

3. Advantages of Belle and Belle II for rare decays

Belle and Belle II have low background environments, with good particle identification and performance. For example, the muon and kaon identification efficiencies are $\sim 90\%$ with $6 - 7\%$ of pion fake-rate. Similarly, the electron identification efficiency is $\sim 86\%$ with $\sim 0.4\%$ of pion fake-rate. In addition to that, we have high photon detection efficiency.

Reconstruction of tag side B (B_{tag}) allows to infer the properties of the signal side B (B_{sig}) with missing energy, and also to have good control over the background. There are different tagging algorithms, *i.e.*, hadronic, semileptonic and inclusive tagging. The hadronic tagging has a efficiency of $O(0.5\%)$ with signal purity of $\sim 10\%$. Similarly, the semileptonic tagging has efficiency of $O(2\%)$ with $\sim 5\%$ purity. Inclusive tagging has higher background contamination but higher efficiency. Full Event Interpretation (FEI) [3] uses a machine-learning algorithm developed for B_{tag} analyses at Belle and Belle II. It supports both hadronic and semileptonic tagging, reconstructing B

mesons across more than 4000 individual decay channels. The training is performed in a hierarchical manner, *i.e.*, the final-state particles are first reconstructed from detector information, then unstable particles are built up from these particles, and reconstruction of B mesons is performed at the end. For each B_{tag} candidate reconstructed by the FEI, a value of the final multivariate classifier output is assigned, which is distributed between zero and one, representing candidates identified as being background-like and signal-like, respectively.

4. $\mathcal{B}(B \to K^* \ell \ell)$ at Belle II

The decays $B \to K^{(*)} \ell \ell$, $\ell = e$ or μ, involves $b \to s \ell \ell$ quark level transition having SM BR $O(10^{-7})$. One of the important observable here is the test of lepton-flavor universality (LFU), $R_{K^{(*)}}$, defined as the ratio of BR from $B \to K^{(*)} \mu \mu$ to $B \to K^{(*)} ee$. According to the SM, this ratio should be one, as the coupling of the lepton to gauge boson is independent of the flavor [4]. LHCb [5] and Belle [6, 7] results for $R_{K^{(*)}}$ are consistent with the SM expectations. Therefore, LFU can be uniquely tested using Belle II data sample.

Belle II [8] has searched for $B^0 \to K^{*0} \ell \ell$ and $B^+ \to K^{*+} \ell \ell$, $\ell \ell = ee$ or $\mu\mu$ decay channels using 189 fb^{-1} of data sample. We reconstruct K^{*0} from $K^+ \pi^-$. Similarly K^{*+} is reconstructed from $K^+ \pi^0$ and $K_S^0 \pi^+$. The background coming from continuum ($q\bar{q} = u\bar{u}, d\bar{d}, s\bar{s}, c\bar{c}$) and generic B (tag-side B) are suppressed using a multivariate analysis technique, FastBDT [9], which used a number of event shape, vertex quality, and kinematic variables. The optimal cut on the FastBDT output is applied to suppress the background and the remaining events are used for further analysis. The signal yield is extracted by performing 2-dimensional unbinned extended maximum likelihood fit in beam-energy constraint mass (M_{bc}) and energy difference (ΔE);

$$M_{\text{bc}} = \sqrt{(E_{\text{beam}}/c^2)^2 - (p_B/c)^2},$$
$$\Delta E = E_B - E_{\text{beam}},$$

where, E_{beam} is the beam energy, while E_B and p_B are respectively are the energy and momentum of the B candidate. These quantities are calculated in the $e^+ e^-$ center-of-mass (c.m.) frame. We analyse the candidates those satisfies $M_{\text{bc}} > 5.2 \, \text{GeV}/c^2$ and $-0.15 < \Delta E < 0.1 \, \text{GeV}$. The correctly reconstructed signal should peak at known B mass and zero for M_{bc} and ΔE, respectively. The signal enhanced projection plots in terms of M_{bc} for $B \to K^* \mu\mu$ and $B \to K^* ee$ is shown in Figure 2. The signal region is defined as $M_{\text{bc}} \in [5.27, 5.29] \, \text{GeV}/c^2$ and $\Delta E \in [-0.05, 0.05] \, \text{GeV}$. There are 22 ± 6, 18 ± 6, and 38 ± 9 signal events for $B \to K^* \mu\mu$, $B \to K^* ee$, and $B \to K^* \ell \ell$ which corresponds to significance of 4.8σ, 3.6σ, and 5.9σ, respectively. The electron and muon channels have similar performance. The measured branching fractions for the entire q^2, invariant mass square of the lepton pairs, region excluding the charmonium resonances (J/ψ and $\psi(2S)$) and low q^2 region to remove the $B \to K^* \gamma (\to ee)$ background, are

$$\mathcal{B}(B \to K^* \mu^+ \mu^-) = (1.19 \pm 0.31^{+0.08}_{-0.07}) \times 10^{-6},$$
$$\mathcal{B}(B \to K^* e^+ e^-) = (1.42 \pm 0.48 \pm 0.09) \times 10^{-6},$$
$$\mathcal{B}(B \to K^* \ell^+ \ell^-) = (1.25 \pm 0.30^{+0.08}_{-0.07}) \times 10^{-6},$$

here, the first and second uncertainties are statistical and systematic, respectively. The precision of the result is limited by sample size and is compatible with world averages [10].
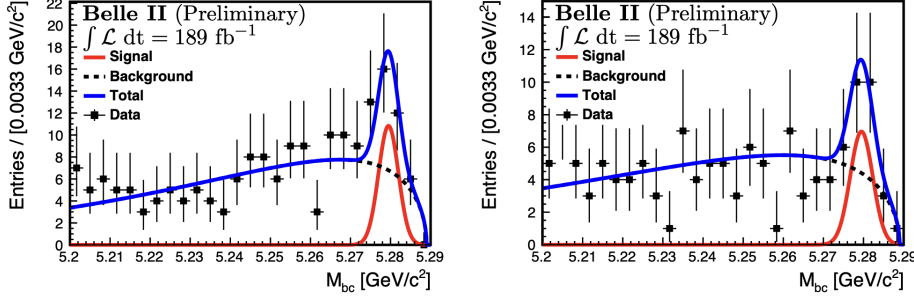
Figure 2: Signal enhanced M_{bc} distributions for $B \to K^*\mu\mu$ (left) and $B \to K^*ee$ (right). Points with error bars are superimposed on the blue (solid) curve, which shows the total fit function, while red (solid) and black (dotted) lines represent the signal and background components, respectively.

5. $\mathcal{B}^{\mathrm{UL}}(B^+ \to K^+\tau^\mp\ell^\pm)$ at Belle

The $b \to s\tau\ell$ and $b \to s\tau\tau$ are expected to be more sensitive to NP which has a coupling proportional to lepton or only couples to the third generation. According to theory, if there is LFU violation there should be lepton-flavor violation (LFV) [11]. The best upper limits (ULs) for LFV $B^+ \to K^+\tau\ell$ and $B^0 \to K^{*0}\tau\mu$ decays are from BaBar [12] and LHCb [13], respectively, which are $O(10^{-5})$. Only $B^+ \to K^+\tau\tau$ decay channel has been searched by BaBar using 342 fb^{-1} data sample and the upper limit is 2.45×10^{-5}, while the SM expectation is $O(10^{-7})$. The $b \to s\tau\tau(\ell)$ are less studied compared to their $e - \mu$ counterparts as they are experimentally challenging due to presence of two or more neutrinos in the final state.

Belle [14] has searched for LFV in $B^+ \to K^+\tau^\mp\ell^\pm$, $\ell = e$ or μ, decays using 711 fb^{-1} data sample. The B_{tag} is reconstructed hadronically using FEI algorithm. The candidate with the highest B_{tag} classifier output is selected and a loose requirement of > 0.001 is applied which rejected significant amount of background and with little signal loss. The signal $B \to K\tau\ell$ decay is searched in the rest of the event, B_{sig}. The τ is reconstructed from $e\overline{\nu}$, $\mu\nu\overline{\nu}$, or $\pi\nu$. The combined branching fraction for these decays is 46%. The $\tau \to \rho\nu$ channel, despite not being explicitly reconstructed, significantly contributes to the $\tau \to \pi\nu$ candidates because of its larger branching fraction ($\sim 25\%$). The dominate background comes from semileptonic D decays *i.e.*, $B^+ \to \overline{D^0}(\to K^+\ell^-\overline{\nu_\ell})X^+$, and semileptonic B decays *i.e.*, $B^+ \to \overline{D^0}(\to K^+X^-)X\ell^+\nu_\ell$. Events compatible with a $B^+_{\mathrm{sig}} \to \overline{D^0}(\to K^+\pi^-)X^+$ decay are rejected by vetoing candidates in the range $1.81 < m_{K^+t^-} < 1.91 \, \mathrm{GeV}/c^2$, where $m_{K^+t^-}$ is the invariant mass of the kaon and oppositely charged particle t^-, that can be the prompt lepton or the τ daughter depending in the charge configuration. Mostly peaking backgrounds are seen for $K\tau\mu$ modes as the probability to identify a pion as a muon is larger than an electron. To further improve the signal selection, BDT classifier is used. Two classifiers are trained for the background suppression. The first one is optimized to reduce the generic B events and uses kinematic information as well as the topology of the B_{sig} and information on the set of ECL clusters that are not used for the B_{sig} and B_{tag} reconstruction. After the optimal cut on first BDT, a large fraction of the surviving background is coming from continuum events. To suppress this background, a second BDT is trained on these events using event shape variables. The

4

optimal cut on the second BDT suppressed remaining continuum events. The $B \to K\tau\ell$ channel has the unique property of having the one or two neutrino coming from the τ itself, allowing the signal yield to be extracted using the recoil mass (M_{recoil}) defined as;

$$M_{\text{recoil}} = \sqrt{m_B^2 + m_{K\ell}^2 - 2(E^*_{\text{beam}}E^*_{K\ell} + p^*_{B_{\text{tag}}}p^*_{K\ell}\cos\theta)},$$

where, θ is the angle between $p^*_{B_{\text{tag}}}$ and $p^*_{K\ell} = (p^*_K + p^*_\ell)$. For correctly reconstructed signal the M_{recoil} should peak at the mass of the τ lepton. There are four decay channels, $B^+ \to K^+\tau^+\mu^-$, $B^+ \to K^+\tau^+e^-$, $B^+ \to K^+\tau^-\mu^+$, and $B^+ \to K^+\tau^-e^+$. The signal yield for $B \to K\tau\ell$ decays are obtained by unbinned extended maximum-likelihood fits to the M_{recoil} distributions. The fit results is shown in Figure 3. The fitted signal yield for different decay channels is consistent with 0. The
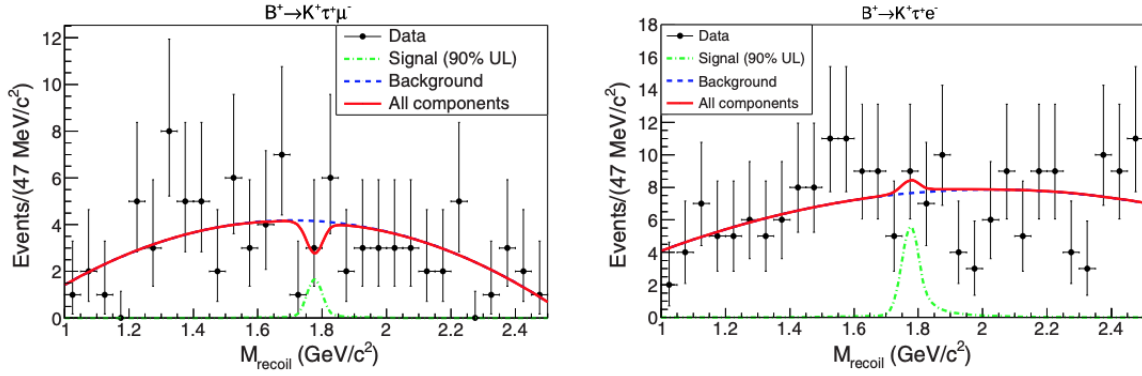

Figure 3: M_{recoil} distribution for the $B^+ \to K^+\tau^+\mu^-$ (left) and $B^+ \to K^+\tau^+e^-$ (right) channels. The black dots show the data, the dashed blue curve shows the background component, and the solid red curve shows the overall fit result. The dash-dotted green curve is the signal PDF, with a normalization corresponding to the 90% CL upper limit.

upper limit (UL) for the modes is calculated at 90% confidence level (CL) using the frequentist approach. The results are summarized in Table 1. These are most stringent upper limits for

channel	N_{sig}	$\mathcal{B}^{\text{UL}}$ (10^{-5})
$B^+ \to K^+\tau^+\mu^-$	-2.1 ± 2.9	< 0.59
$B^+ \to K^+\tau^+e^-$	1.5 ± 5.5	< 1.51
$B^+ \to K^+\tau^-\mu^+$	2.3 ± 4.1	< 2.45
$B^+ \to K^+\tau^-e^+$	-1.1 ± 7.4	< 1.53

Table 1: Fit yields and branching fraction upper limits at the 90% CL for $B \to K\tau\ell$ decay channels.

$B^+ \to K^+\tau^\mp\ell^\pm$ decay channels.

6. $\mathcal{B}^{\text{UL}}(B^0 \to K^{*0}\tau\tau)$ at Belle

Belle [15] has searched for the rare $B^0 \to K^{*0}\tau\tau$ decays using 711 fb^{-1} data sample. In this search we fully reconstruct the companion B meson produced in the process $e^+e^- \to \Upsilon(4S) \to B\bar{B}$

from its hadronic decay modes, and look for the decay $B^0 \to K^{*0}\tau^+\tau^-$ in the rest of the event. A candidate B_{tag} meson is reconstructed in one of the 489 hardonic decay channels using a hierarchical neural network (NN). In this algorithm, the continuum background are suppressed by employed event shape variables. The combinatorial background is suppressed using some minimum criteria on the output of the NN. With this, the remaining backgrounds are mostly from generic B in which a B_{tag} is properly reconstructed opposite $B^0 \to D^-\ell^+\nu_\ell$ decaying to $D^- \to K^{*0}\ell^-\overline{\nu_\ell}$. Such events have the same final-state particles as signal events, the only difference is the number of missing neutrinos resulting in different missing mass distribution, M_{miss}. A cut of $M_{\text{miss}}^2 < 9 \text{ GeV}^2/c^4$ is applied to reject these backgrounds. The signal side τ is reconstructed from $e^-\overline{\nu_e}\nu_\tau$, $\mu^-\overline{\nu_\mu}\nu_\tau$, and $\pi^-\nu_\tau$. There are 6 different decay channels, *i.e.*, $K^{*0}e^+e^-$, $K^{*0}e^\mp\mu^\pm$, $K^{*0}\mu^+\mu^-$, $K^{*0}\pi^\mp e^\pm$, $K^{*0}\pi^\mp\mu^\pm$, $K^{*0}\pi^+\pi^-$. In the signal decay channels $K^{*0}\pi^+\pi^-$ and $K^{*0}\ell^\pm\pi^\mp$, there remains a large background contribution from the decay $B^0 \to D^{(*)-}\ell^+\nu_\ell$, where $D^{(*)-} \to K^{*0}\pi^-(\pi^0)$ and is suppressed by requiring the invariant mass $M_{K^{*0}\pi^-}$ to lie outside the D^- mass region, *i.e.*, $M_{K^{*0}\pi^-} < 1.84 \text{ GeV}/c^2$ or $M_{K^{*0}\pi^-} > 1.94 \text{ GeV}/c^2$ where $M_{K^{*0}\pi^-}$ is the combination of the K^{*0} candidate and a track that is opposite to the charge of the kaon candidate in the K^{*0} decay. The signal yield is extracted with a binned extended maximum-likelihood fit to the extra calorimetric energy distribution, $E_{\text{ECL}}^{\text{extra}}$, with a bin width of 0.1 GeV. The fit result for all decay channels combined is shown in Figure 4. The
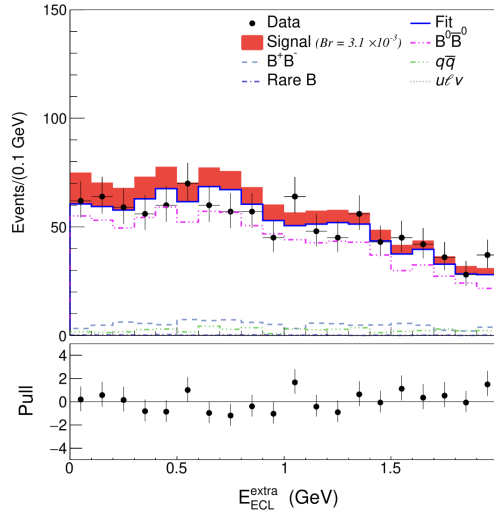

Figure 4: Distribution of $E_{\text{ECL}}^{\text{extra}}$ combined for all signal channels. The dots with error bars show the data, the blue line shows the fitted results with the background-only model, and the dashed lines show fit results for the different components. A signal (red region) with a branching fraction of 3.1×10^{-3}, corresponding to the upper limit at 90% CL, is superimposed on the top of the fit.

numbers of signal and background events in the signal window, $[0, 0.2]$ GeV, are -4.9 ± 6.0 and 122.4 ± 4.9, respectively, obtained from the fit. We find no evidence for the signal. The signal yield obtained from the extended maximum likelihood fit is translated into an UL on the $B^0 \to K^{*0}\tau^+\tau^-$ branching fraction using the CL_s method [16, 17]. The observed upper limit on the branching fraction is 3.1×10^{-3} at 90% CL. This is the first experimental limit on the decay $B^0 \to K^{*0}\tau^+\tau^-$.

7. Inclusive $\mathcal{B}(B \to X_s \gamma)$ at Belle II

Belle II [18] has measured the photon-energy spectrum in radiative B decays into inclusive final states involving a strange hadron and a photon using 189 fb^{-1} data sample. These FCNC processes are particularly sensitive to non-SM effects [19]. In addition, their photon-energy spectrum offers access to various interesting parameters, such as the mass of the b quark and the function describing its motion inside the B meson. In the inclusive measurement using $B \to X_s \gamma$ decays identified in $\Upsilon(4S) \to B\overline{B}$ events in which the partner B meson is reconstructed in its hadronic decays using FEI algorithm. The tagging provides a purer sample and the kinematic information from the partner B-meson gives direct access to observables in the signal-B meson rest frame. Due to the high-purity of the tagged sample, background contamination is low at high photon-candidate energy in the signal-B meson rest-frame, E_γ^B, but grows sharply with decreasing E_γ^B, shown in Figure 5. The tag-side M_{bc} distribution is fitted in bins of E_γ^B to extract the signal yield. The sample
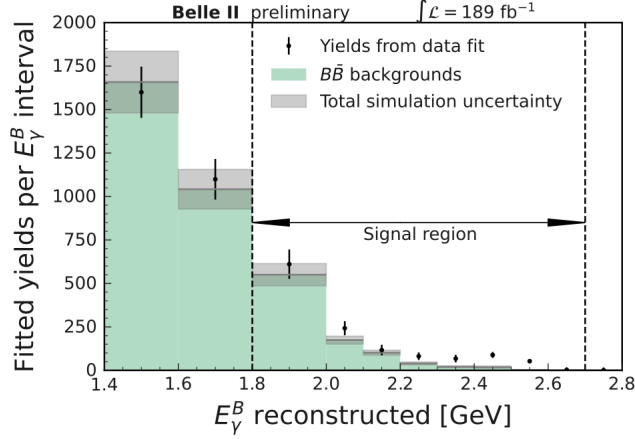

Figure 5: Yield of generic B events as a function of photon energy in the signal B meson rest frame. The histogram shows the luminosity-scaled yields from the background-only simulated sample. The gray bands correspond to systematic uncertainties on the generic B predicted.

is divided in 11 bins: three 200 MeV wide bins for the $1.4 - 2.0$ GeV range; seven 100 MeV bins for the $2.0 - 2.7$ GeV region; and a single $E_\gamma^B > 2.7$ GeV bin. The first two bins and the last one are chosen as control regions for the fit due to expected large background or low signal yield. The signal region is therefore defined as $1.8 < E_\gamma^B < 2.7$ GeV. The inclusive analysis doesn't distinguish between contributions from $b \to d\gamma$ and $b \to s\gamma$ processes, therefore the much smaller $b \to d\gamma$ contribution is accounted for by assuming same shape and efficiency as signal but suppressed by a factor of $|V_{td}/V_{ts}|^2 \sim 4.3\%$. The background from continuum events is suppressed using a BDT trained with event shape variables. The fit to tag-side M_{bc} distribution for $1.8 < E_\gamma^B < 2.0$ GeV bin is shown in left plot of Figure 6. The resulting partial branching fractions are shown in right plot of Figure 6. The inclusive branching ratio $\mathcal{B}(B \to X_s \gamma)$ for various E_γ^B thresholds is given in Table 2. The results are consistent with the SM and world averages [10].
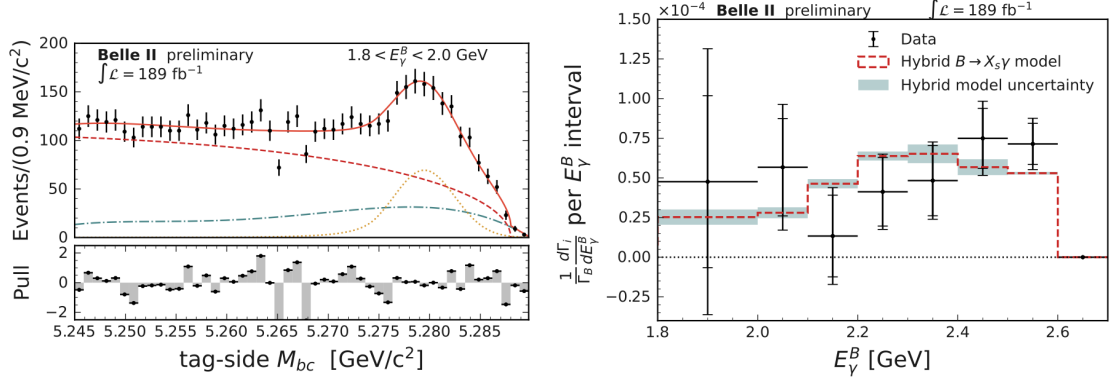
Figure 6: The left plot shows the distribution of tag-side B meson $M_{\rm bc}$ for the E_γ^B bin of $[1.8, 2.0]$ GeV. The orange dotted curve corresponds to the generic B peaking tags. The dashed and dash-dotted curves correspond to the continuum and misreconstructed generic B components. The solid red curve is the total fit. The right plot is the measured partial branching fraction $(1/\Gamma_B)(d\Gamma_i/dE_\gamma^B)$ as a function of E_γ^B. The outer (inner) uncertainty bar shows the total (statistical) uncertainty. The overlaid model and uncertainty corresponds to the hybrid model.

E_γ^B threshold [GeV]	$\mathcal{B}(B \to X_s\gamma)$ (10^{-4})
1.8	$3.54 \pm 0.78 \pm 0.83$
2.0	$3.06 \pm 0.56 \pm 0.47$
2.1	$2.49 \pm 0.46 \pm 0.35$

Table 2: Integrated partial branching fractions for three E_γ^B thresholds.

8. Exclusive $\mathcal{B}(B \to \rho\gamma)$ at Belle and Belle II

$b \to d\gamma$ transition have an order of magnitude lower branching fraction compared to $b \to s\gamma$ process. The $B \to \rho\gamma$ decay can be affected by NP that does not appear in $b \to s$ processes, $B \to \rho\gamma$ decays have been observed by the Belle [22, 23] and BaBar [24] experiments. The current world average of isospin asymmetry is about two standard deviation from the SM expectation.

The measurements of $B \to \rho\gamma$ decays using a combined data sample of 772×10^6 $B\overline{B}$ pairs collected by the Belle experiment and 387×10^6 $B\overline{B}$ pairs collected by the Belle II experiment [20]. We reconstruct both charged and neutral B, where $\rho^0 \to \pi^+\pi^-$ and $\rho^+ \to \pi^+\pi^0$. To suppress the contribution from continuum background, a BDT is used containing event shape variables. To extract physics observables, a simulatneous fit is performed to the $M_{\rm bc}$, ΔE, and $M_{K\pi}$ distributions with an extended unbinned maximum likelihood method to six independent data sets: B^+, B^-, and B^0 in Belle and Belle II. Here, $M_{K\pi}$ is defined as the invariant mass of the ρ candidate calculated assuming that one of the charged pions is a kaon; for the $\rho^0 \to \pi^+\pi^-$ decay, the redefinition of the mass hypothesis is applied to the charged π with the lowest probability of being a pion, and this variable helps separate $K^*\gamma$ background better compared to $M_{\pi\pi}$. The projections of the fit results in terms of ΔE is shown in Figure 7. The branching fractions, direct CP asymmetry, and isospin
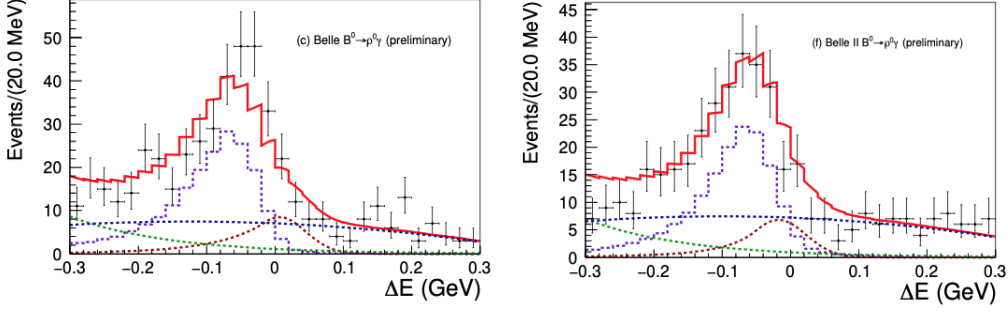
Figure 7: Distributions of ΔE for $B^0 \to \rho^0 \gamma$ candidates reconstructed in the signal enhanced region, $M_{\rm bc} > 5.27$ GeV/c^2 and $M_{K\pi} > 0.92$ GeV/c^2 in Belle (left) and Belle II (right) data. The points with error bars are data, the solid red curves are the sum of signal and background PDFs, the dashed red curves are signal, the dotted blue curves are continuum background, the dashed yellow curves are $K^*\gamma$ background, and the dotted-dashed green curve are generic B background other than $K^*\gamma$ background.

asymmetry results are

$$\mathcal{B}(B^+ \to \rho^+ \gamma) = (13.1^{+2.0+1.3}_{-1.9-1.2}) \times 10^{-7},$$
$$\mathcal{B}(B^0 \to \rho^0 \gamma) = (7.5 \pm 1.3^{+1.0}_{-0.8}) \times 10^{-7},$$
$$A_{CP}(B^+ \to \rho^+ \gamma) = (-8.2 \pm 15.2^{+1.6}_{-1.2})\%,$$
$$A_I(B \to \rho\gamma) = (10.9^{+11.2+6.8+3.8}_{-11.7-6.2-3.9})\%,$$

where, the first uncertainty is statistical, the second is systematic, and the third for A_I is the uncertainty from f^{+-}/f^{00} along with the lifetime ratio of B^+ and B^0. The improved result for A_I is consistent with the SM within 0.6σ. All measurements are the most precise to date. The results supersede the previous measurements performed by Belle [21].

9. Summary

In summary, Belle has most stringent upper limits on branching fraction for lepton-flavor violating $B^+ \to K^+ \tau^\mp \ell^\pm$ decays at 90% CL are $< (0.59 - 2.45) \times 10^{-5}$. The first experimental limit on the decay $B^0 \to K^{*0}\tau\tau$ is $< 3.1 \times 10^{-3}$ at 90% CL using full data sample of Belle. Belle II is heading towards the test of lepton-flavor universality. So far we have measured the branching fraction of $B \to K^*\ell\ell$ using 189 fb^{-1} data sample and the results are consistent with the PDG. The branching fraction measurement for inclusive $B \to X_s\gamma$ decays for different photon energy thresholds, E^B_γ, are consistent with world averages. We have world's most precise measurement of $B \to \rho\gamma$ decays branching fraction, isospin asymmetry, and CP-asymmetry using data samples from Belle and Belle II.

Belle II will restart data taking from early 2024, and we will have many exciting results on rare decays.

References

[1] A. Abashian *et al.* (Belle Collaboration), NIMPRS A **479** (2002) 117; also, see the detector section in J. Brodzicka *et al.*, PTEP **2012** (2012) 04D001.

[2] T. Abe *et al.* (Belle II Collaboration), arXiv:1011.0352.

[3] T. Keck *et al.* (Belle II Collaboration), CSBS **3** (2019) 6.

[4] M. Bordone *et al.*, EPJC **76** (2016) 440.

[5] R. Aaij *et al.* (LHCb Collaboration), PRL **131** (2023) 051803.

[6] S. Choudhury *et al.* (Belle Collaboration), JHEP **03** (2021) 105.

[7] S. Wehle *et al.* (Belle Collaboration), PRL **126** (2021) 161801.

[8] F. Abudinén *et al.* (Belle II Collaboration), arXiv:2206.05946.

[9] T. Kech, arXiv:1609.06119.

[10] R. L. Workman *et al.* (Particle Data Group), PTEP **2022** (2022) 083C01.

[11] S. L. Glashow *et al.*, PRL **114** (2015) 091801.

[12] J. P. Lees *et al.* (BaBar Collaboration), PRD **86** (2012) 012004.

[13] A. Aaij *et al.* (LHCb Collaboration), JHEP **06** (2023) 143.

[14] S. Watanuki *et al.* (Belle Collaboration), PRL **130** (2023) 261802.

[15] T. V. Dong *et al.* (Belle Collaboration), PRD **108** (2023) L01102.

[16] A. L. Read, J. Phys. G **28** (2002) 2693.

[17] G. Cowan, K. Cranmer, E. Gross, and O. Vitells, EPJC **71** (2011) 1554; EPJC **73** (2013) 2501 (E).

[18] F. Abudinén *et al.* (Belle II Collaboration), arXiv: 2210.10220.

[19] M. Misiak *et al.*, EPJC **77** (2017) 201.

[20] Belle II Collaboration, EPS HEP 2023.

[21] N. Taniguchi *et al.* (Belle Collaboration), PRL **101** (2008) 111801.

[22] D. Mohapatra *et al.* (Belle Collaboration), PRL **96** (2006) 221601.

[23] N. Taniguchi *et al.* (Belle Collaboration), PRL 101 (2008) 111801.

[24] B. Aubert *et al.* (BaBar Collaboration), PRD **78** (2008) 112001.